


Investigation of chemical noise in multisite phosphorylation chain using linear noise approximationSoutrick Das  and Debashis Barik **School of Chemistry, University of Hyderabad, Gachibowli, 500046, Hyderabad, India* (Received 12 July 2019; revised manuscript received 24 October 2019; published 11 November 2019)

Quantitative and qualitative nature of chemical noise propagation in biochemical reaction networks depend crucially on the topology of the networks. Multisite reversible phosphorylation-dephosphorylation of target proteins is one such recurrently found topology that regulates host of key functions in living cells. Here we analytically calculated the stochasticity in multistep reversible chemical reactions by determining variance of phosphorylated species at the steady state using linear noise approximation to investigate the effect of mass action and Michaelis-Menten kinetics on the noise of phosphorylated species. We probed the dependence of noise on the number of phosphorylation sites and the equilibrium constants of the reaction equilibria to investigate the chemical noise propagation in the multisite phosphorylation chain.

DOI: [10.1103/PhysRevE.100.052402](https://doi.org/10.1103/PhysRevE.100.052402)**I. INTRODUCTION**

An isogenic population of cells in identical environmental conditions show remarkable population heterogeneity in protein abundance, cell cycle properties, cell size and shape, and timescales of key signaling events [1–7]. The observed population heterogeneity was found to be due to the intrinsic and extrinsic sources of noise that ultimately are responsible for stochastic trajectories of chemical reactions inside living cells [8]. These sources of fluctuations are called chemical noise. While intrinsic noise originates from the fluctuations of molecular species with finite abundance and leads to stochastic trajectories of chemical species over time; extrinsic noise originates from the variation of the global factors such as cell volume or size, cell cycle phases, abundances of regulatory molecules (e.g., transcription factors). Although intrinsic noise influences the outcome of a particular reaction but extrinsic noise affects all the chemical reactions equally in a given cell [9]. In many situations chemical noise may act as nuisance for a number of physiological processes; however, it also plays beneficial roles in a number of cellular functions [10–12].

Using probabilistic description of chemical reactions, theoretical and computational models of gene expression noise were able to quantitatively explain many experimental observations on protein noise [13–15]. However, cellular functions are regulated by chemical reaction networks involving many genes. Often these networks consist of small regulatory network motifs with distinct steady-state and dynamical properties [16]. Therefore, further investigations were carried out to understand the effects of network topologies such as signaling cascades, feedback loops and feed-forward loops on the propagation of chemical noise [17–23]. Multisite reversible phosphorylation-dephosphorylation of proteins is one such network motif that regulate catalytic activity, binding, transport, and degradation of target proteins [24,25]. For

example, many crucial events in eukaryotic cell cycle are regulated by multisite phosphorylations of several key proteins by cyclin-dependent kinase [26]. Phosphorylation or dephosphorylation can occur either in processive or distributive manner. In processive mechanism, a single encounter between the enzyme and the substrate results attachment of multiple phosphate groups to the substrate. Whereas, in the distributive mechanism a single encounter results in a single enzymatic event. When the same enzyme catalyzes multiple phosphorylation in a distributive manner, it leads to ultrasensitive signal response—a requirement for generating nonlinear responses in biochemical reaction networks [24,27–29]. Therefore, multisite phosphorylation mechanism has been widely used in mathematical and computational modeling of bistability and oscillations [30–35]. Although various facets of multisite phosphorylation have been studied in the context of its deterministic dynamics [24,27,29,33,34], however systematic investigation of stochasticity in multiphosphorylation is lacking. Therefore, it is crucial to study the characteristics of chemical noise in multisite phosphorylation chain. In particular, it is worth investigating the dependence of intrinsic noise in multiphosphorylation chain on the rate laws of chemical reactions, kinetic parameters and total number of phosphorylation sites.

Keeping in view of the important role of multisite phosphorylation, we investigated propagation of intrinsic noise in multisite phosphorylation chain with different “chain lengths,” i.e., with different total number of phosphorylation sites on the target protein. Further we explored both mass action (MA) and Michaelis-Menten (MM) rate laws for phosphorylation and dephosphorylation reactions to determine the effect of nonlinearity on noise propagation. To investigate the quantitative and qualitative nature of variability in phosphorylated species, we used van Kampens system size expansion method which is also known as linear noise approximation (LNA) to the chemical master equation [36]. Further, we supplemented our analytical calculations with stochastic simulations of chemical reactions in the chain using Gillespie’s stochastic simulation algorithm (SSA) [37].

*dbariksc@uohyd.ac.in

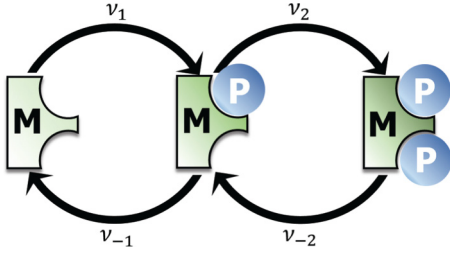


FIG. 1. Schematic diagram of three-component phosphorylation-dephosphorylation chain. v_i and v_{-i} represent the macroscopic rates of phosphorylation and dephosphorylation reactions, respectively.

II. MODEL AND METHOD

We studied noise propagation in ordered distributive multisite phosphorylation where each enzyme-substrate encounter leads to single phosphorylation or dephosphorylation of target protein with a specific order [29]. In Fig. 1, we present a reaction scheme of a three-component multisite phosphorylation-dephosphorylation chain. In our scheme an enzyme (kinase) catalyzes all the phosphorylation events and similarly another enzyme (phosphatase) catalyzes all the dephosphorylation events. The chemical master equation of the three component reaction scheme can be represented as [38]:

$$\begin{aligned} \frac{\partial p(n_0, n_1, n_2; t)}{\partial t} &= a_1(n_0 + 1, n_1 - 1, n_2)p(n_0 + 1, n_1 - 1, n_2; t) \\ &+ a_2(n_0, n_1 + 1, n_2 - 1)p(n_0, n_1 + 1, n_2 - 1; t) \\ &+ a_{-2}(n_0, n_1 - 1, n_2 + 1)p(n_0, n_1 - 1, n_2 + 1; t) \\ &+ a_{-1}(n_0 - 1, n_1 + 1, n_2)p(n_0 - 1, n_1 + 1, n_2; t) \\ &- [a_1(n_0, n_1, n_2) + a_2(n_0, n_1, n_2) + a_{-2}(n_0, n_1, n_2) \\ &+ a_{-1}(n_0, n_1, n_2)]p(n_0, n_1, n_2; t), \end{aligned} \quad (1)$$

where $p(n_0, n_1, n_2; t)$ is the joint probability distribution that at time t , there are n_0 , n_1 , and n_2 number of molecules of unphosphorylated (MP_0), singly phosphorylated (MP_1), and doubly phosphorylated (MP_2) species, respectively. The a_i 's are the reaction propensities for phosphorylation (a_1, a_2) or dephosphorylation (a_{-1}, a_{-2}) reaction steps in the chain. As mass conservation law holds in the chain, the total number of molecules, $n_T (= n_0 + n_1 + n_2)$, is fixed at all time. The chemical master equation can also be written as a function of any two variables of the phosphorylation chain due to the mass conservation [39].

For the three component chain, the equations for the average dynamics of the phosphorylated species are given by

$$\frac{\partial \bar{n}_1}{\partial t} = v_1 + v_{-2} - v_2 - v_{-1}, \quad (2a)$$

$$\frac{\partial \bar{n}_2}{\partial t} = v_2 - v_{-2}, \quad (2b)$$

where \bar{n}_1 and \bar{n}_2 are the macroscopic average of MP_1 and MP_2 , respectively. v_i and v_{-i} represent the macroscopic rates of phosphorylation and dephosphorylation reactions. This set of equations essentially represent the macroscopic rate equations resulted from the deterministic chemical kinetics of

the well-mixed reacting system. Using mass conservation one can obtain the average population of the unphosphorylated species. MM rate laws have been used widely to model the dynamics of multisite phosphorylation reactions. Particularly the relevance of the MM rate laws in multisite phosphorylation has become quite significant since the work of Markevich *et al.* [28] in the context of mitogen-activated protein kinase pathway. Their work has established that, in certain conditions, a three-component phosphorylation-dephosphorylation cycle alone can generate bistability without any imposed positive feedback loop in the reaction network. However, a two-component phosphorylation-dephosphorylation cycle with MM kinetics leads to ultrasensitive switch [40]. Further various aspects of ultrasensitive switch by multisite phosphorylation with MM kinetics have been investigated [27]. In addition to the MM kinetics, MA based multisite phosphorylation was also shown to generate robust and tunable ultrasensitivity [29]. With the consideration that both MA and MM kinetics are equally important in producing nonlinear responses, we investigated chemical noise propagation in multisite phosphorylation with both types of rate laws.

A. Mass action kinetics

We assumed that the chemical reactions in the multisite phosphorylation chain follow the MA rate laws of chemical kinetics. Assumption of MA rate law in the enzymatic step demands that the initial encounter between the enzyme and the substrate is the rate limiting step of the reaction. The reaction propensities, v_i , are given by

$$v_1 = k_1(n_T - \bar{n}_1 - \bar{n}_2), \quad (3a)$$

$$v_2 = k_2\bar{n}_1, \quad (3b)$$

$$v_{-1} = k_{-1}\bar{n}_1, \quad (3c)$$

$$v_{-2} = k_{-2}\bar{n}_2, \quad (3d)$$

where \bar{n}_i is the average number of molecules for the i th chemical species. In the above set of equations, the k_i and k_{-i} are the catalytic conversion rate constants for phosphorylation (k_1, k_2) and dephosphorylation (k_{-1}, k_{-2}) reactions, respectively. We kept the abundances of enzymes constant in the entire calculations. Therefore, they are not mentioned explicitly as they were absorbed in the rate constants k_i and k_{-i} . Although we have presented the dynamical equations for a three-component system, however, the general form of the dynamical equations and macroscopic rates can be written for any component chain (See Eqs. (A1)–(A3) in the Appendix).

To calculate the steady-state fluctuations in phosphospecies we used LNA on the chemical master equation. The method relies on the system size (Ω) expansion of the master equation [36]. Identifying Ω as the volume of the reaction chamber of the homogeneous reaction mixture, the main *ansatz* in the system size expansion is that the sizes of the fluctuations from the macroscopic average varies inversely with $\sqrt{\Omega}$. Systematic expansion of the chemical master equation to the first order in $1/\sqrt{\Omega}$ leads to equations for the averages. Whereas the expansion to the second order in $1/\sqrt{\Omega}$ results in a linear Fokker-Planck equation of the relevant random variables. Since in the process of generating Fokker-Planck equation, higher order terms above $1/\Omega^0$ are excluded, it is

called linear noise approximation. In the past, this method has been used extensively to calculate gene expression noise and noise in biochemical reaction networks [14,41–43]. Further LNA has been applied in case of autocatalytic system [44], in two-component signal transduction pathway [45], reactions with nonlinear rate laws [46–48] and spatial systems [49]. The applicability of LNA has been tested extensively in the various contexts of biochemical systems [50,51] and the method has been extended to systems with nonunique stationary states with multistability [52], with extrinsic noise [53] and systems with disparate timescales [54].

Owing to the linearity of the Fokker-Planck equation obtained from the LNA, the drift and diffusion matrices are connected by a fluctuation-dissipation-like relation at the steady state:

$$\mathbf{A}\sigma + \sigma\mathbf{A}^T + \mathbf{B} = \mathbf{0}. \quad (4)$$

In the fluctuation-dissipation relation above, \mathbf{A} , \mathbf{B} , and σ are the drift (or Jacobian matrix), diffusion, and covariance matrix, respectively. The covariance matrix holds information about the steady-state variance and covariance of all the molecular species in the network. The elements in the drift matrix \mathbf{A} are given by

$$A_{ij} = \frac{\partial}{\partial \bar{n}_j} \frac{\partial \bar{n}_i}{\partial t}. \quad (5)$$

Note that, for simplicity we are using the same notation for steady-state averages (\bar{n}_i) as we used for the non-steady-state quantities represented in Eq. (2). The elements in the diffusion matrix \mathbf{B} are given by

$$B_{ij} = \sum_k v_{jk} v_{ik} v_k, \quad (6)$$

where v_{ik} is the stoichiometric coefficient of the i th species in the k th reaction, and v_k is the rate of the k th reaction.

Here we assumed mass conservation ($n_T = \sum n_i$) to reduce the number of variables. Consequently the drift and diffusion matrices depend only on the average population of phosphorylated species (\bar{n}_1 and \bar{n}_2). Now for the MA kinetics Eq. (3) the drift and diffusion matrices are given by

$$\mathbf{A} = \begin{bmatrix} -(k_1 + k_2 + k_{-1}) & (k_{-2} - k_1) \\ k_2 & -k_{-2} \end{bmatrix}, \quad (7)$$

$$\mathbf{B} = \begin{bmatrix} 2(k_2 + k_{-1})\bar{n}_1 & -2k_2\bar{n}_1 \\ -2k_2\bar{n}_1 & 2k_{-2}\bar{n}_2 \end{bmatrix}. \quad (8)$$

Using the above expressions of \mathbf{A} and \mathbf{B} in the fluctuation-dissipation relation Eq. (4) and applying the symmetry of the elements of the covariance matrix ($\sigma_{ij} = \sigma_{ji}$) we obtained a matrix equation for the steady-state second moments of the random variables:

$$\begin{bmatrix} \sum_{i=1}^2 k_i + k_{-1} & k_1 - k_{-2} & 0 \\ k_2 & -\sum_{i=1}^2 (k_i + k_{-i}) & k_{-2} - k_1 \\ 0 & k_2 & -k_{-2} \end{bmatrix} \begin{bmatrix} \sigma_{11} \\ \sigma_{12} \\ \sigma_{22} \end{bmatrix} = \begin{bmatrix} -(k_2 + k_{-1})\bar{n}_1 \\ 2k_2\bar{n}_1 \\ -k_{-1}\bar{n}_2 \end{bmatrix}. \quad (9)$$

Solution of the above system of linear equations leads to the steady-state variances of singly and doubly phosphorylated species MP_1 and MP_2 , respectively, and are given as

$$\sigma_{11} = \frac{(k_1 k_2 + k_{-1} k_{-2}) \bar{n}_1}{k_1 k_2 + k_1 k_{-2} + k_{-1} k_{-2}}, \quad (10a)$$

$$\sigma_{22} = \frac{(k_1 k_{-2} + k_{-1} k_{-2}) \bar{n}_2}{k_1 k_2 + k_1 k_{-2} + k_{-1} k_{-2}}. \quad (10b)$$

The above set of equations can be used to compute the dependence of variances of phosphorylated species on the various rate parameters in the reaction scheme. In the special case, where all the forward and backward rate constants are equal, i.e., $k_1 = k_2 = k_f$ and $k_{-1} = k_{-2} = k_b$, the steady-state variances can be represented as a function of ratio of catalytic conversion rates, $K (= k_f/k_b)$, and they take simple forms as

$$\sigma_{11} = \frac{(1 + K^2) \bar{n}_1}{(1 + K)^2 - K}, \quad (11a)$$

$$\sigma_{22} = \frac{(1 + K) \bar{n}_2}{(1 + K)^2 - K}. \quad (11b)$$

The macroscopic steady-state averages (\bar{n}_i) can be obtained from the deterministic dynamical Eqs. (2). In the above mentioned special case, the general expression of the average of the i th phosphospecies is given as

$$\bar{n}_i = \frac{K^i}{\sum_{i=0}^N K^i} n_T. \quad (12)$$

N is the total number of phosphorylation sites in the chemical species. For the two-component phosphorylation chain the steady-state variance for MP_1 can be obtained following the method described as above and is given as

$$\sigma_{11} = \frac{\bar{n}_1}{(K + 1)}. \quad (13)$$

B. Michealis-Menten kinetics

Next, we investigate the case where phosphorylation and dephosphorylation reactions are governed by the Michaelis-Menten rate laws. For the three-component phosphorylation chain (Fig. 1) the mathematical expressions of macroscopic rates, v_i , are given as

$$v_1 = \frac{k_1 E_1 (n_T - \bar{n}_1 - \bar{n}_2) / K_{M1}}{1 + (n_T - \bar{n}_1 - \bar{n}_2) / K_{M1} + \bar{n}_1 / K_{M2}}, \quad (14a)$$

$$v_2 = \frac{k_2 E_1 \bar{n}_1 / K_{M2}}{1 + (n_T - \bar{n}_1 - \bar{n}_2) / K_{M1} + \bar{n}_1 / K_{M2}}, \quad (14b)$$

$$v_{-1} = \frac{k_{-1} E' \bar{n}_1 / K_{-M1}}{1 + \bar{n}_1 / K_{-M1} + \bar{n}_2 / K_{-M2}}, \quad (14c)$$

$$v_{-2} = \frac{k_{-2} E' \bar{n}_2 / K_{-M2}}{1 + \bar{n}_1 / K_{-M1} + \bar{n}_2 / K_{-M2}}. \quad (14d)$$

These rate expressions are similar to expressions as given by Markovich *et al.* [28] in the context of phosphorylation of mitogen-activated protein kinase cascade. E_1 and E' are the kinase and phosphatase abundances, respectively, and we kept their abundances constant throughout the calculations. The K_{M_i} 's are the Michaelis constants for phosphorylation (K_{M1} , K_{M2}) and dephosphorylation (K_{-M1} , K_{-M2}) reactions.

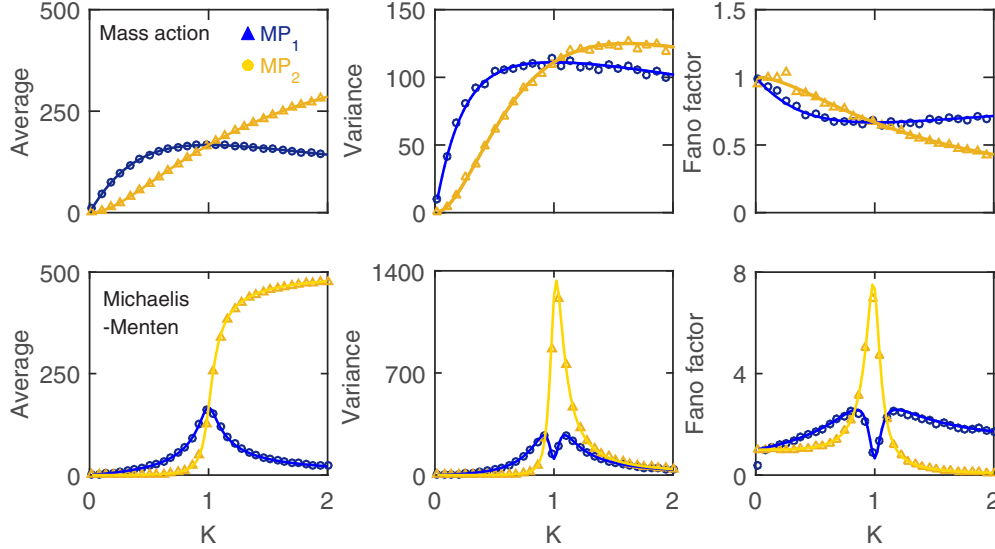


FIG. 2. Dependence of steady-state statistical properties (average (\bar{n}_i), variance (σ_{ii}), and Fano factor (σ_{ii}/\bar{n}_i)) on the equilibrium constant (K) for phosphorylation-dephosphorylation reactions in three component multiphosphorylation chain. Solid lines and markers represent analytical and SSA simulation results, respectively. $n_T = 500$ was chosen in all the calculations. Top row: mass action kinetics; bottom row: Michaelis-Menten kinetics.

We followed the same general method, as described in the case of MA kinetics to obtain the matrix equation for the covariances of phosphorylated species. The final matrix equation for the covariances is given as

$$\begin{bmatrix} A_{11} & A_{12} & 0 \\ A_{12} & (A_{11} + A_{22}) & A_{12} \\ 0 & A_{12} & A_{22} \end{bmatrix} \begin{bmatrix} \sigma_{11} \\ \sigma_{12} \\ \sigma_{22} \end{bmatrix} = \begin{bmatrix} -\frac{1}{2}(v_1 + v_2 + v_{-2} + v_{-1}) \\ (v_2 + v_{-2}) \\ -\frac{1}{2}(v_2 + v_{-2}) \end{bmatrix}. \quad (15)$$

The matrix elements for the \mathbf{A} can be represented as

$$A_{11} = -\frac{\frac{E_1}{K_{M1}K_{M2}}[(k_1K_{M2} + k_2K_{M1}) + (k_1 + k_2)(n_T - \bar{n}_2)]}{X_1} - \frac{\frac{E'}{K_{-M1}K_{-M2}}[k_{-1}K_{-M2} + (k_{-1} + k_{-2})\bar{n}_2]}{X_2}, \quad (16a)$$

$$A_{12} = \frac{\frac{E'}{K_{-M1}K_{-M2}}[k_{-2}K_{-M1} + (k_{-1} + k_{-2})\bar{n}_1]}{X_2}, \quad (16b)$$

$$A_{21} = \frac{\frac{E_1}{K_{M1}K_{M2}}[k_2K_{M1} + k_2(n_T - \bar{n}_2)]}{X_1} + \frac{\frac{E'}{K_{-M1}K_{-M2}} \cdot k_{-2}\bar{n}_2}{X_2}, \quad (16c)$$

$$A_{22} = \frac{\frac{E'}{K_{-M1}K_{-M2}}[k_{-2}K_{-M1} + k_{-2}\bar{n}_1]}{X_2}, \quad (16d)$$

with $X_1 = [1 + (n_T - \bar{n}_1 - \bar{n}_2)/K_{M1} + \bar{n}_1/K_{M2}]^2$ and $X_2 = [1 + \bar{n}_1/K_{-M1} + \bar{n}_2/K_{-M2}]^2$. Due to the nonlinear nature of the rate functions, the elements in the matrix \mathbf{A} are cumbersome in their appearance. Consequently the analytical solution of σ_{ii} cannot be expressed in simple forms. Therefore, to obtain the variances of phosphorylated species, we used MATLAB to solve the matrix Eq. (15). However, for the two-component phosphorylation-dephosphorylation

cycle, the steady-state variance for MP_1 can be expressed as

$$\sigma_{11} = \frac{\frac{k_1 E (n_T - \bar{n}_1)}{K_{M1} + (n_T - \bar{n}_1)} + \frac{k_{-1} E' \bar{n}_1}{K_{-M1} + \bar{n}_1}}{\frac{2k_1 E K_{M1}}{[K_{M1} + (n_T - \bar{n}_1)]^2} + \frac{2k_{-1} E' K_{-M1}}{[K_{-M1} + \bar{n}_1]^2}}. \quad (17)$$

C. Results

In the quest of determining the steady-state statistical properties of phosphorylated species, in Fig. 2 we present the dependence of average, variance, and Fano factor of the phosphorylated species on the equilibrium constant (K) of phosphorylation-dephosphorylation reactions in the three-component phosphochain. To understand the effect of the rate laws on the statistical properties, we report results both from the MA and the MM kinetics of reactions. Further, to test the accuracy of our analytical calculations, we compared the analytical results with the results from numerical simulations performed using Gillespie's SSA. In the case of MA kinetics, we used Eqs. (11) and (12) for variance and average, respectively. Whereas, in the case of MM kinetics, we solved the matrix Eq. (15) in MATLAB to obtain the variances. Although we report results for the cases with $k_1 = k_2$ and $k_{-1} = k_{-2}$, however, one can also get the dependence of statistical properties on the individual rate constants (k_1 , k_2 , k_{-1} , and k_{-2}). In MA kinetics, with the increase of K ($= k_1/k_{-1} = k_2/k_{-2}$) the variances of the phosphorylated states increase sharply and decreases steadily passing through maxima. Whereas in the case of MM kinetics the increase and decrease of variances are much sharper. Particularly for the terminally phosphorylated species (MP_2) the variance exhibits a sharp peak at $K = 1$. The sharp rise of variance of MP_2 is due to rapid increase of its average near $K = 1$. However, the rapid fall of variance beyond $K > 1$ is due to decrease in sizes of fluctuations as the species are entirely converted to MP_2 at large value of K . As in the MA kinetics, the averages do not show such sharp transition with K the corresponding variances also do not

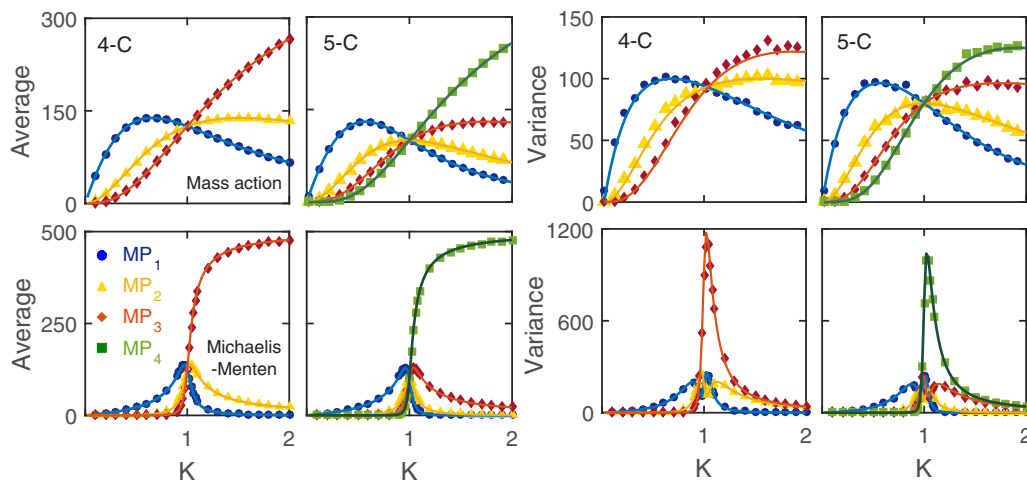


FIG. 3. Variation of steady-state average and variance with the equilibrium constant (K) in four (4-C) and five (5-C) component multiphosphorylation chains. Solid lines and markers represent analytical and numerical results, respectively. Top row: mass action kinetics; bottom row: Michaelis-Menten kinetics. To vary K , we kept $k_b (= k_{-1} = k_{-2})$ fixed at 0.2 and varied $k_f (= k_1 = k_2)$. The values of all Michaelis constants were fixed at 0.05. The parameters were $n_T = 500$, $E = 50$, and $E' = 50$.

exhibit sharp features. Therefore, well-known ultrasensitive switching of MP_2 dictates the behavior of its variance. The variation of Fano factor ($=$ variance/mean), that measures the strength of the noise, also supports the dependence of variance on K . Further the deviation of Fano factor from 1 indicates the non-Poissonian nature of statistics across different values of K .

Many regulatory proteins that control key cellular functions are often phosphorylated multiple times and often it results in ultrasensitive signal response curves. Particularly the sharpness in the signal response strongly depends on the number of phosphorylation of the target protein [29]. Keeping in view with this, we next investigated phosphochains with four- and five-components. To get the steady-state variances, we followed the method described earlier. The dynamical equations and rate functions for MA and MM kinetics are given in the Appendix [Eqs. (A1)–(A3)]. Further, the corresponding matrix equations for the steady-state covariances are also given in the Appendix [Eqs. (A4) and (A5) for MA kinetics and Eqs. (A6) and (A7) for MM kinetics]. As the dimension of these matrix equations are large, obtaining analytical expressions of the variances (σ_{ii}) are quite difficult. Thus we again resort to MATLAB to get the solution of these matrix equations. In Fig. 3 we present the variation of the steady-state averages and variances of the phosphorylated species with the equilibrium constant K . Similar to the three-component chain, in the case of MA kinetics the variances increase and decrease less dramatically as compared to the MM kinetics. Again the terminally phosphorylated species exhibit sharp rise and fall in its variance in MM kinetics - owing to its deterministic behavior. We also support our analytical results with the numerical calculations using Gillespie's SSA. Both the results agree very well in all chains. Further, it is interesting to note that all the variance curves cross through a common value of $K = 1$ in MA kinetics.

Now that we have established our method, next we investigated the effect of chain lengths or the total number of phosphorylation sites (N) on the variability of phosphorylated

species. We calculated the coefficient of variation ($CV =$ standard deviation/mean) to estimate the noise in the chemical species. We calculated CV of all the phosphorylated species in chains having 3, 4, and 5 components and in all chains we kept the total number of species fixed at $n_T = 500$. We then compared the CV of a given phosphorylated state from different chain lengths (Fig. 4) to assess the effect of number of phosphorylation sites on the noise. Our calculations indicate that, in the case of MA kinetics the noise in a particular phosphorylated state increases with the chain length. This is due to the fact that the total population is distributed over all the states, thus the average abundance of a particular state decreases with the chain length resulting in higher noise in the individual phosphorylated states. While the CV of the terminally phosphorylated species in any chain exhibit monotonously decreasing trend with the K , however, the CV of other phosphorylated species pass through a minimum. The reason for monotonous decrease of CV with K for the terminally phosphorylated species is the increase of average abundance with the K . However, with K , average abundances of other phosphorylated species pass through maxima and consequently the CV of these species follow a reverse trend. Although these findings are also generally true for the MM kinetics, however, near the critical value of $K = 1$ the CV exhibits a sudden dip for the nonterminal phosphorylated species. For the terminal species, the CV decreases sharply at $K = 1$ as compared to the MA kinetics—again due to the average dynamics. Further the noise in the MM kinetics is more for the nonterminal species as compared to the MA kinetics. To get a better estimate of comparative noise in MA and MM kinetics, we calculated the total variance of all the phosphorylated species and compared them for chains of different number of components (Fig. 5). While in the case of MA kinetics, the total variance increases with the number of components in the chain, however, the total variance of all the chains are nearly same in the case of MM kinetics. More importantly the total variance in the MM kinetics is much higher than that of in the MA kinetics. This indicates

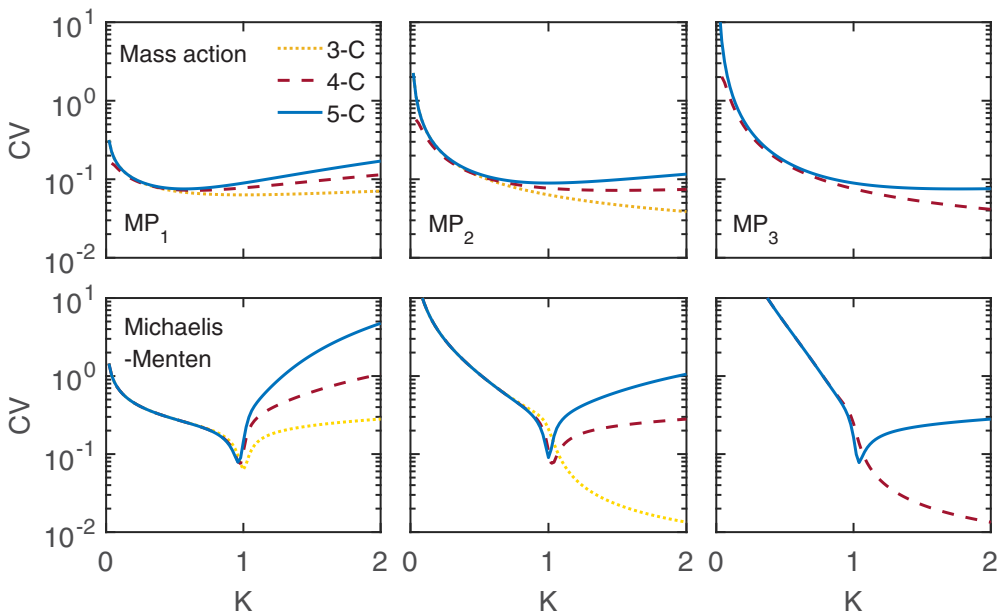


FIG. 4. Comparison of noise (coefficient of variation, $CV = \sqrt{\sigma_{ii}/n_i}$) of given phosphorylated species from chains of different sizes. Different colors or line styles represent different chains.

that nonlinear rates in the chemical kinetics contributes to amplify the intrinsic noise in the phosphorylation chains. Therefore, although nonlinear rate laws results in sharp ultrasensitive response, however, it also increases the variability in the phosphostates in the reaction equilibria.

Propagation of chemical noise in a network of chemical reactions has been of a great interest since the inception of gene expression noise. A particular interest has been signaling cascade network where the propagation of intrinsic noise has been investigated as a function of cascade “length” [17,55–58]. Therefore, in the case of multisite phosphorylation chain, it is a reasonable to determine how the noise is distributed or propagated among the various chemical species in the chain. In addition, it is worth determining the effect of chain

length *i.e.* the number of components in the phosphorylation chain on the noise of phosphorylated species. To address these aspects of noise propagation, we performed additional simulations for longer phosphorylation chains all the way up to 10 components. In Fig. 6 we report the noise propagation along the different chains at $K = 1$. Particularly, for a given chain, we plot the noise of all the phosphorylated species both for MA and MM kinetics. We found a striking difference in the noise propagation between chains with MA and MM rate laws. In the MA kinetics, the noise of all the phosphorylated species of a chain are same. However, the quantitative value

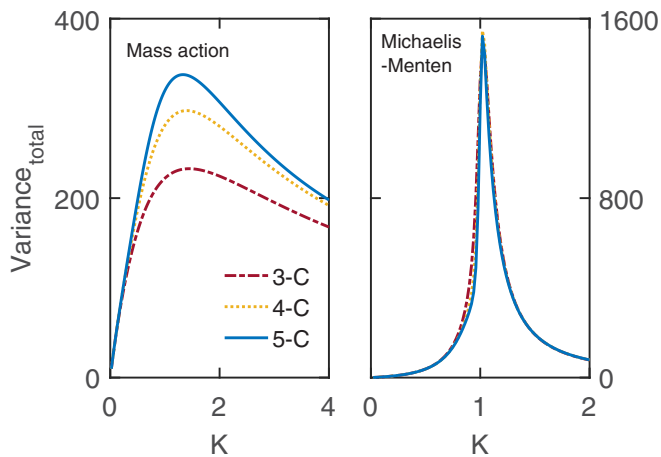


FIG. 5. Total variance ($= \sum_{ii} \sigma_{ii}$) of all phosphorylated species of each multiphosphorylation chain is plotted against the equilibrium constant. Each color or line style represents chain with different number of components.

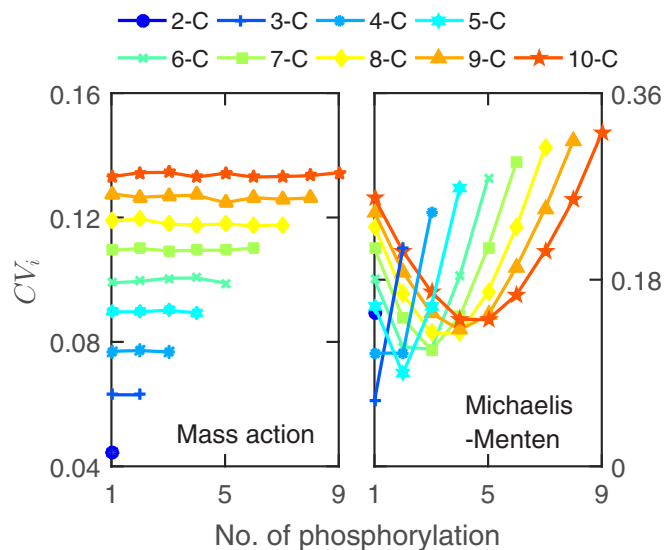


FIG. 6. Plot of coefficient of variation (CV_i) for all the phosphorylated species in a given chain as a function of number of phosphorylation for MA (left) and MM (right) kinetics for $K = 1$. The different colors or point styles represent different chain lengths.

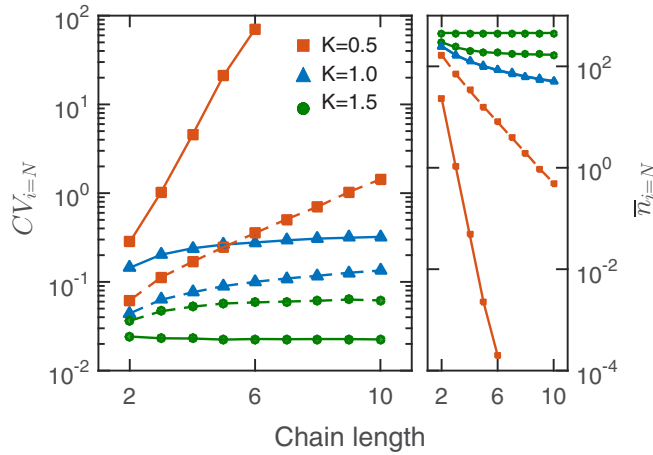


FIG. 7. Variation of CV (left panel) and average (right panel) for terminally phosphorylated species (MP_N) with the chain length for indicated values of K . Dashed and solid lines correspond to MA and MM kinetics, respectively.

of noise depends on the chain length where longer chains are more noisy than shorter chains. Therefore, the extent of noise propagation is independent of the phosphorylation state of the species. Whereas in the case of MM kinetics, the noise exhibits a completely different qualitative behavior. Here the noise is somewhat parabolic in nature with the phosphorylation state of the species. The noise decreases with the phosphorylation and passing through a minimum it further increases along the chain. Therefore, the “middle” of the chains are least noisy than the “terminals” of the chain.

To determine how the noise of a given species depends on the chain length, in Fig. 7 we report the CV of the terminal phosphorylated species (MP_N) as a function of chain “length” for three different values of K . When dephosphorylation reactions are favored over the phosphorylation reactions ($K = 0.5$), the noise in the terminal phosphorylated

species increases with the chain length due to the decreased average abundance of species with chain length. At $K = 1$ both phosphorylation and dephosphorylation are equally favored and the noise increases steadily with the chain length. Finally, when phosphorylation is favored over dephosphorylation ($K = 1.5$), the noise remains same for most of the chains due to the full saturation of terminally phosphorylated species that has a bound in terms of maximum abundance (fixed N_T). Further, one important aspect to note that, the noise in the terminally phosphorylated species is more in MM kinetics as compared to MA kinetics for $K = 0.5$ and $K = 1$. Whereas the situation is the opposite in the case of $K = 1$.

One of the important aspects of intrinsic noise is that the dependence of CV on the average number of molecular species. For simple birth-death processes, the CV follows its characteristic $CV \propto 1/\sqrt{\bar{n}}$ scaling behavior. In Fig. 8 we present the dependence of CV on the average abundance of phosphorylated species for chains with different total number of phosphorylation sites. In the case of MA kinetics, the CV shows usual scaling with the average number of species ($CV \propto 1/\sqrt{\bar{n}}$) and the CVs for all the phosphorylated species behave identically with the average. However, the scaling of CV in the MM kinetics is complex in nature. Particularly the intermediate phosphorylated species show a looplike feature which is characteristic to MM kinetics of enzymatic reaction. This characteristic feature of noise versus abundance may be useful for the experimentalists to determine the mechanism of enzymatic activity particularly whether the underlying rate law was MM or MA kinetics.

III. CONCLUSION

Chemical reactions in living cells experience unavoidable intrinsic noise that originates from fluctuations of the finite abundance of molecular species. Due to the chemical noise expression of gene becomes noisy [1,2]. The ultimate end result of noisy gene expression is population

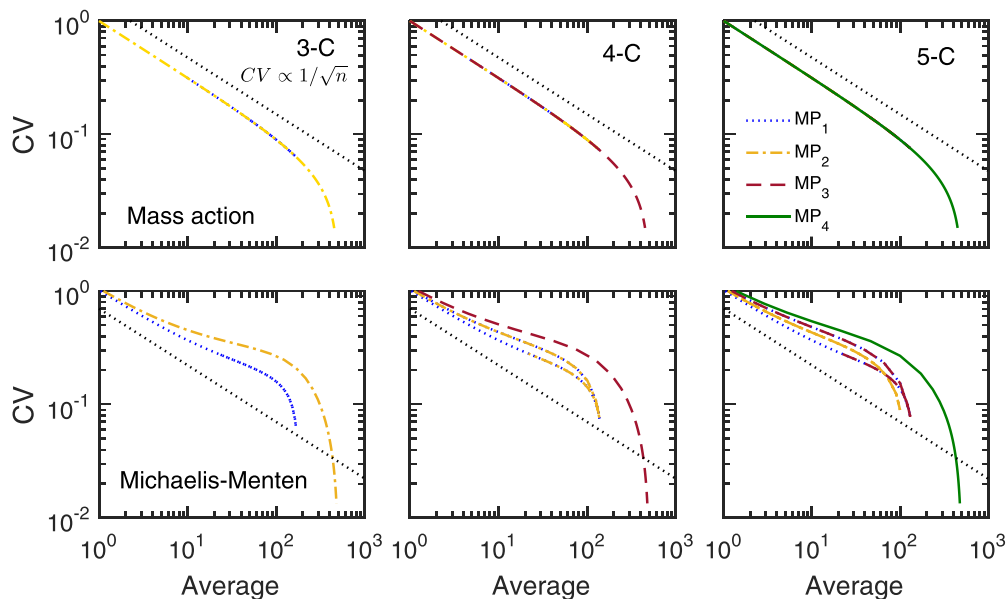


FIG. 8. CV vs average plots for phosphostates in each chain (3, 4, and 5 component). Different colors or line styles represent each phosphorylated species. The dotted lines across the plot represent $CV \propto 1/\sqrt{N}$ scaling.

heterogeneity of cellular functions or characteristics. The topology of reaction network is a key regulator of chemical noise propagation in biochemical reaction networks that control diverse cellular functions. Multisite phosphorylation of protein is one such network motif that is often responsible for activation, inactivation, recognition, binding, degradation of many target proteins. Further it is also found to be responsible for ultrasensitive response in signaling networks. Therefore, understanding of chemical noise propagation in a chain of multisite phosphorylation reactions is important due to its variety of roles in cellular signaling. In this paper, we analytically investigated chemical noise propagation in multisite phosphorylation chains using van Kampens system size expansion method. We have supplemented the analytical results with numerical simulations of chemical reactions using Gillespie's SSA. To understand the role of rate laws in noise propagation, we carried out calculations with both linear (mass action) and nonlinear (Michaelis-Menten) kinetics for the enzymatic activity. We calculated steady-state statistical properties (variance, coefficient of variation, Fano factor) of phosphorylated species while we varied the equilibrium constant of phosphorylation-dephosphorylation reaction and the total number of phosphorylated states in the chain (chain length) to study noise propagation.

In the case of MA kinetics, the variance of phosphorylated states increase and decrease steadily with the equilibrium constant of the reactions. However, in the case of MM kinetics, the rise and fall of variances are much profound. Particularly the variance of the terminally phosphorylated species exhibits a sharp peak at $K = 1$ where the reaction equilibrium is unbiased. Further the variance of any phosphorylated state with the MM kinetics is significantly larger than that of with the MA kinetics. Consequently the total variance in all the phosphostates with the MM kinetics is much higher than the total variance in the MA kinetics. This is also reflected in the CV that estimates the "noisiness" of the chemical species. It is established that MM kinetics in multiphosphorylation chain can lead to ultrasensitive signal response. Goldbeter-Koshland's zero-order ultrasensitive switch in a two-component phosphorylation-dephosphorylation chain is an example of such ultrasensitivity [40]. Our calculations indicate that although MM kinetics leads to increased sharpness in the signal response, however, it contributes to the amplification of variability of the phosphorylated states as compared to the MA kinetics. Therefore, it is a trade off for the system that achieves sharp nonlinear response, however, at the cost of increased variability. Our investigations on the propagation of intrinsic noise along the chain unravel a stark contrast by which chemical noise propagates along the chains with MA or MM kinetics. Where in MA kinetics the noise is independent of the state of the phosphorylation, the noise

crucially depends on the state of phosphorylation in the MM kinetics. In particular the noise varies in a parabolic manner along the chain. Further in both the kinetics, the noise of terminal phosphospecies increases steadily with the length of the chain at $K = 1$. Finally, the CV versus average plots indicate that in the MA kinetics the system follows $CV \propto 1/\sqrt{N}$ irrespective of the state of the phosphorylation. In the MM kinetics, on the contrary, it does not exhibit similar the scaling relation. Further the distinctive loop structure in the CV versus average plot of intermediate phosphorylated states can be useful to determine the underlying rate law of enzymatic events in phosphorylation-dephosphorylation reaction chain.

ACKNOWLEDGMENTS

The work of D.B. was supported by funding from the Science and Engineering Research Board, Department of Science and Technology (India), Grant No. EMR/2015/001899. S.D. acknowledges fellowship from INSPIRE program of Department of Science and Technology (India).

APPENDIX: MATRIX EQUATIONS FOR THE STEADY-STATE COVARIANCES

General deterministic dynamical equations for the multiphosphorylation chain with N number of phosphorylation sites. The number of components will be $N + 1$:

$$\frac{\partial \bar{n}_i}{\partial t} = (v_i + v_{-(i+1)}) - (v_{(i+1)} + v_{-i}), \quad (\text{A1a})$$

$$\frac{\partial \bar{n}_N}{\partial t} = (v_N - v_{-N}). \quad (\text{A1b})$$

For the MA kinetics the general form of macroscopic rates are given as

$$v_i = k_i \bar{n}_{i-1}, \quad (\text{A2a})$$

$$v_{-i} = k_{-i} \bar{n}_i. \quad (\text{A2b})$$

For the MM kinetics the general form of the macroscopic rates are given as

$$v_i = \frac{k_i E (\bar{n}_{i-1} / K_{Mi})}{1 + \sum_{i=1}^N (\bar{n}_{i-1} / K_{Mi})}, \quad (\text{A3a})$$

$$v_{-i} = \frac{k_{-i} E' (\bar{n}_i / K_{-Mi})}{1 + \sum_{i=0}^{N-1} (\bar{n}_{i+1} / K_{-Mi})}. \quad (\text{A3b})$$

The matrix equation for covariances of the phosphorylated species in the four-component phosphorylation chain with MA rate law is represented as

$$\begin{bmatrix} -p_4 & q_4 & -k_1 & 0 & 0 & 0 \\ k_2 & -(p_4 + r_4) & k_{-3} & q_4 & -k_1 & 0 \\ 0 & k_3 & -(p_4 + k_{-3}) & 0 & q_4 & -k_1 \\ 0 & k_2 & 0 & -r_4 & k_{-3} & 0 \\ 0 & 0 & k_2 & k_3 & -(r_4 + k_{-3}) & k_{-3} \\ 0 & 0 & 0 & 0 & k_3 & -k_{-3} \end{bmatrix} \begin{bmatrix} \sigma_{11} \\ \sigma_{12} \\ \sigma_{13} \\ \sigma_{21} \\ \sigma_{22} \\ \sigma_{33} \end{bmatrix} = \begin{bmatrix} -(k_2 + k_{-1}) \bar{n}_1 \\ (k_2 \bar{n}_1 + k_{-2} \bar{n}_2) \\ 0 \\ -(k_3 + k_{-2}) \bar{n}_2 \\ 2k_3 \bar{n}_2 \\ -k_{-3} \bar{n}_3 \end{bmatrix}, \quad (\text{A4})$$

where $p_4 = k_1 + k_2 + k_{-1}$, $q_4 = k_{-2} - k_1$, and $r_4 = k_3 + k_{-2}$.

The matrix equation for covariances of the phosphorylated species in the five-component phosphorylation chain with MA rate law is represented as

$$\begin{bmatrix} -p_5 & q_5 & -k_1 & -k_1 & 0 & 0 & 0 & 0 & 0 & 0 \\ k_2 & -(p_5 + r_5) & k_{-3} & 0 & q_5 & -k_1 & -k_1 & 0 & 0 & 0 \\ 0 & k_3 & -(p_5 + s_5) & k_{-4} & 0 & q_5 & 0 & -k_1 & -k_1 & 0 \\ 0 & 0 & k_4 & -(p_5 + k_{-4}) & 0 & 0 & q_5 & 0 & -k_1 & -k_1 \\ 0 & k_2 & 0 & 0 & -r_5 & k_{-3} & 0 & 0 & 0 & 0 \\ 0 & 0 & k_2 & 0 & k_3 & -(r_5 + s_5) & k_{-4} & k_{-3} & 0 & 0 \\ 0 & 0 & 0 & k_2 & 0 & k_4 & -(r_5 + k_{-4}) & 0 & k_{-3} & 0 \\ 0 & 0 & 0 & 0 & 0 & k_3 & 0 & -s_5 & k_{-4} & 0 \\ 0 & 0 & 0 & 0 & 0 & 0 & k_3 & k_4 & -(s_5 + k_{-4}) & k_{-4} \\ 0 & 0 & 0 & 0 & 0 & 0 & 0 & 0 & k_4 & -k_{-4} \end{bmatrix} \begin{bmatrix} \sigma_{11} \\ \sigma_{12} \\ \sigma_{13} \\ \sigma_{14} \\ \sigma_{22} \\ \sigma_{23} \\ \sigma_{24} \\ \sigma_{33} \\ \sigma_{34} \\ \sigma_{44} \end{bmatrix} = \begin{bmatrix} -(k_2 + k_{-1})\bar{n}_1 \\ k_2\bar{n}_1 + k_{-2}\bar{n}_2 \\ 0 \\ 0 \\ -(k_3 + k_{-2})\bar{n}_2 \\ k_3\bar{n}_2 + k_{-3}\bar{n}_3 \\ 0 \\ -(k_4 + k_{-3})\bar{n}_3 \\ 2k_4\bar{n}_3 \\ -k_{-4}\bar{n}_4 \end{bmatrix}, \tag{A5}$$

where $p_5 = k_1 + k_2 + k_{-1}$, $q_5 = k_{-2} - k_1$, $r_5 = k_3 + k_{-2}$, and $s_5 = k_4 + k_{-3}$. These matrix equations can be solved in MATLAB to get the variances of the phosphorylated species.

The matrix equation for covariances of the phosphorylated species in the four-component phosphorylation chain with MM rate law is represented as

$$\begin{bmatrix} A_{11} & A_{12} & A_{13} & 0 & 0 & 0 \\ A_{21} & (A_{11} + A_{22}) & A_{23} & A_{12} & A_{13} & 0 \\ A_{31} & A_{32} & (A_{11} + A_{33}) & 0 & A_{12} & A_{13} \\ 0 & A_{21} & 0 & A_{22} & A_{23} & 0 \\ 0 & A_{31} & A_{21} & A_{32} & (A_{22} + A_{33}) & A_{23} \\ 0 & 0 & A_{31} & 0 & A_{32} & A_{33} \end{bmatrix} \begin{bmatrix} \sigma_{11} \\ \sigma_{12} \\ \sigma_{13} \\ \sigma_{22} \\ \sigma_{23} \\ \sigma_{33} \end{bmatrix} = \begin{bmatrix} -\frac{1}{2}(v_1 + v_2 + v_{-1} + v_{-2}) \\ (v_2 + v_{-2}) \\ 0 \\ -\frac{1}{2}(v_2 + v_3 + v_{-2} + v_{-3}) \\ (v_3 + v_{-3}) \\ -\frac{1}{2}(v_3 + v_{-3}) \end{bmatrix}. \tag{A6}$$

The matrix equation for the five-component chain with MM rate law is given as

$$\begin{bmatrix} A_{11} & A_{12} & A_{13} & A_{14} & 0 & 0 & 0 & 0 & 0 & 0 \\ A_{21} & (A_{11} + A_{22}) & A_{23} & A_{24} & A_{12} & A_{13} & A_{14} & 0 & 0 & 0 \\ A_{31} & A_{32} & (A_{11} + A_{33}) & A_{34} & 0 & A_{12} & 0 & A_{13} & A_{14} & 0 \\ A_{41} & A_{42} & A_{43} & (A_{11} + A_{44}) & 0 & 0 & A_{12} & 0 & A_{13} & A_{14} \\ 0 & A_{21} & 0 & 0 & A_{22} & A_{23} & A_{24} & 0 & 0 & 0 \\ 0 & A_{31} & A_{21} & 0 & A_{32} & (A_{22} + A_{33}) & A_{34} & A_{23} & A_{24} & 0 \\ 0 & A_{41} & 0 & A_{21} & A_{42} & A_{43} & (A_{22} + A_{44}) & 0 & A_{23} & A_{24} \\ 0 & 0 & A_{31} & 0 & 0 & A_{32} & 0 & A_{33} & A_{34} & 0 \\ 0 & 0 & A_{41} & A_{31} & 0 & A_{42} & A_{32} & A_{43} & (A_{33} + A_{44}) & A_{34} \\ 0 & 0 & 0 & A_{41} & 0 & 0 & A_{42} & 0 & A_{43} & A_{44} \end{bmatrix} \begin{bmatrix} \sigma_{11} \\ \sigma_{12} \\ \sigma_{13} \\ \sigma_{14} \\ \sigma_{22} \\ \sigma_{23} \\ \sigma_{24} \\ \sigma_{33} \\ \sigma_{34} \\ \sigma_{44} \end{bmatrix} = \begin{bmatrix} -\frac{1}{2}(v_1 + v_2 + v_{-1} + v_{-2}) \\ (v_2 + v_{-2}) \\ 0 \\ 0 \\ -\frac{1}{2}(v_2 + v_3 + v_{-2} + v_{-3}) \\ (v_3 + v_{-3}) \\ 0 \\ -\frac{1}{2}(v_3 + v_4 + v_{-3} + v_{-4}) \\ (v_4 + v_{-4}) \\ -\frac{1}{2}(v_4 + v_{-4}) \end{bmatrix}. \tag{A7}$$

Considering the forms of these matrix equations for four- and five-component chains, it is possible to generalize the matrix equation for a chain of any number of components. However, it is difficult to represent the generalized matrix equation in a simple format.

-
- [1] E. M. Ozbudak, M. Thattai, I. Kurtser, A. D. Grossman, and A. van Oudenaarden, *Nat. Genet.* **31**, 69 (2002).
- [2] M. B. Elowitz, A. J. Levine, E. D. Siggia, and P. S. Swain, *Science* **297**, 1183 (2002).
- [3] D. E. Nelson, A. E. C. Ihekweba, M. Elliott, J. R. Johnson, C. A. Gibney, B. E. Foreman, G. Nelson, V. See, C. A. Horton, D. G. Spiller, S. W. Edwards, H. P. McDowell, J. F. Unitt, E. Sullivan, R. Grimley, N. Benson, D. Broomhead, D. B. Kell, and M. R. H. White, *Science* **306**, 704 (2004).
- [4] N. Geva-Zatorsky, N. Rosenfeld, S. Itzkovitz, R. Milo, A. Sigal, E. Dekel, T. Yarnitzky, Y. Liron, P. Polak, G. Lahav, and U. Alon, *Mol. Syst. Biol.* **2**, 2006.0033 (2006).
- [5] S. Di Talia, J. M. Skotheim, J. M. Bean, E. D. Siggia, and F. R. Cross, *Nature* **448**, 947 (2007).
- [6] O. Feinerman, J. Veiga, J. R. Dorfman, R. N. Germain, and G. Altan-Bonnet, *Science* **321**, 1081 (2008).
- [7] B. Cerulus, A. M. New, K. Pougach, and K. J. Verstrepen, *Curr. Biol.* **26**, 1138 (2016).
- [8] A. Raj and A. van Oudenaarden, *Cell* **135**, 216 (2008).
- [9] P. S. Swain, M. B. Elowitz, and E. D. Siggia, *Proc. Natl. Acad. Sci. USA* **99**, 12795 (2002).
- [10] A. Eldar and M. B. Elowitz, *Nature* **467**, 167 (2010).
- [11] M. Ackermann, *Nat. Rev. Microbiol.* **13**, 497 (2015).
- [12] M. K. Jolly, P. Kulkarni, K. Weninger, J. Orban, and H. Levine, *Front. Oncol.* **8**, 50 (2018).
- [13] M. Thattai and A. van Oudenaarden, *Proc. Natl. Acad. Sci. USA* **98**, 8614 (2001).
- [14] J. Paulsson, *Nature* **427**, 415 (2004).
- [15] T. Jia and R. V. Kulkarni, *Phys. Rev. Lett.* **106**, 058102 (2011).
- [16] J. J. Tyson and B. Novák, *Annu. Rev. Phys. Chem.* **61**, 219 (2010).
- [17] J. Pedraza and A. van Oudenaarden, *Science* **307**, 1965 (2005).
- [18] O. Brandman, *Science* **310**, 496 (2005).
- [19] B. Ghosh, R. Karmakar, and I. Bose, *Phys. Biol.* **2**, 36 (2005).
- [20] F. J. Bruggeman, N. Blüthgen, and H. V. Westerhoff, *PLoS Comput. Biol.* **5**, e1000506 (2009).
- [21] D. Barik, D. A. Ball, J. Peccoud, and J. J. Tyson, *PLoS Comput. Biol.* **12**, e1005230 (2016).
- [22] S. R. Chepyala, Y.-C. Chen, C.-C. S. Yan, C.-Y. D. Lu, Y.-C. Wu, and C.-P. Hsu, *Sci. Rep.* **6**, 23607 (2016).
- [23] A. Dey and D. Barik, *PLOS ONE* **12**, e0188623 (2017).
- [24] C. Salazar and T. Höfer, *FEBS J.* **276**, 3177 (2009).
- [25] C. Conradi and A. Shiu, *Biophys. J.* **114**, 507 (2018).
- [26] R. J. Deshaies and J. E. Ferrell, *Cell* **107**, 819 (2001).
- [27] J. Gunawardena, *Proc. Natl. Acad. Sci. USA* **102**, 14617 (2005).
- [28] N. I. Markevich, J. B. Hoek, and B. N. Kholodenko, *J. Cell Biol.* **164**, 353 (2004).
- [29] O. Kapuy, D. Barik, M. R. Domingo Sananes, J. J. Tyson, and B. Novak, *Prog. Biophys. Mol. Biol.* **100**, 47 (2009).
- [30] L. Yang, W. R. MacLellan, Z. Han, J. N. Weiss, and Z. Qu, *Biophys. J.* **86**, 3432 (2004).
- [31] G. Yao, T. J. Lee, S. Mori, J. R. Nevins, and L. You, *Nat. Cell Biol.* **10**, 476 (2008).
- [32] D. Barik, W. T. Baumann, M. R. Paul, B. Novak, and J. J. Tyson, *Mol. Syst. Biol.* **6**, 405 (2010).
- [33] M. Thomson and J. Gunawardena, *Nature* **460**, 274 (2009).
- [34] J. E. Ferrell, Jr. and S. H. Ha, *Trends Biochem. Sci.* **39**, 556 (2014).
- [35] C. Conradi and M. Mincheva, *J. R. Soc., Interface* **11**, 20140158 (2014).
- [36] N. van Kampen, *Stochastic Processes in Physics and Chemistry*, 3rd ed. (Elsevier, Amsterdam, 2007).
- [37] D. T. Gillespie, *J. Comput. Phys.* **22**, 403 (1976).
- [38] C. Gardiner, *Stochastic Methods: A Handbook for the Natural and Social Sciences*, 4th ed. (Springer, Berlin, 2009).
- [39] J. Paulsson, *Phys. Life Rev.* **2**, 157 (2005).
- [40] A. Goldbeter and D. E. Koshland, *Proc. Natl. Acad. Sci. USA* **78**, 6840 (1981).
- [41] J. Elf and M. Ehrenberg, *Genome Res.* **13**, 2475 (2003).
- [42] F. Hayot and C. Jayaprakash, *Phys. Biol.* **1**, 205 (2004).
- [43] H. El-Samad and M. Khammash, *Biophys. J.* **90**, 3749 (2006).
- [44] C. Cianci, F. Di Patti, D. Fanelli, and L. Barletti, *Eur. Phys. J.: Spec. Top.* **212**, 5 (2012).
- [45] A. K. Maity, A. Bandyopadhyay, P. Chaudhury, and S. K. Banik, *Phys. Rev. E* **89**, 032713 (2014).
- [46] J. Elf, J. Paulsson, O. G. Berg, and M. Ehrenberg, *Biophys. J.* **84**, 154 (2003).
- [47] X. Zheng and Y. Tao, *Phys. Chem. Chem. Phys.* **12**, 2418 (2010).
- [48] X. Zheng and Y. Tao, *J. Chem. Phys.* **128**, 165104 (2008).
- [49] P. Lötstedt, *Bull. Math. Biol.* **81**, 2873 (2018).
- [50] P. Thomas, H. Matuschek, and R. Grima, *BMC Genom.* **14**, S5 (2013).
- [51] R. Grima, *Phys. Rev. E* **92**, 042124 (2015).
- [52] P. Thomas, N. Popović, and R. Grima, *Proc. Natl. Acad. Sci. USA* **111**, 6994 (2014).
- [53] E. M. Keizer, B. Bastian, R. W. Smith, R. Grima, and C. Fleck, *Phys. Rev. E* **99**, 052417 (2019).
- [54] P. Thomas, A. V. Straube, and R. Grima, *BMC Syst. Biol.* **6**, 39 (2012).
- [55] S. Hooshangi, S. Thiberge, and R. Weiss, *Proc. Natl. Acad. Sci. USA* **102**, 3581 (2005).
- [56] M. Thattai and A. van Oudenaarden, *Biophys. J.* **82**, 2943 (2002).
- [57] V. Dhananjayulu, V. N. Sagar P, G. Kumar, and G. A. Viswanathan, *PLoS One* **7**, 1 (2012).
- [58] D. A. Oyarzn, J.-B. Lugagne, and G.-B. V. Stan, *ACS Synth. Biol.* **4**, 116 (2015).